5th GRACM International Congress on Computational Mechanics
Limassol, 29 June – 1 July, 2005

ANALYTICAL MODELING OF ELASTOMERIC LEAD-RUBBER BEARINGS WITH THE USE OF FINITE ELEMENT MICROMODELS

I.N. Doudoumis*, F. Gravalas*, N.I. Doudoumis*

* Department of Civil Engineering
Aristotle University of Thessaloniki (A.U.Th.)
54006 Thessaloniki, GREECE,
e-mail: doud@civil.auth.gr

Keywords: Lead Rubber Bearings, Finite element micromodels, Analytical modeling, Base isolation.

Abstract. *The simplified models used for the simulation of the mechanical behavior of the Lead-Rubber Bearings (LRBs) are not always sufficiently accurate. The current paper attempts to certify the accuracy of the simplified models by comparing their mechanical behavior with the behavior of proper finite-element micromodels. The LRBs consist of two mounting steel plates located at the top and bottom of the bearing, several alternating layers of elastomer and steel shims and a central lead core. In the paper, the geometric shape of these bearings is modeled analytically with sufficient accuracy by taking into account detailed fabrication drawings of a standard LRB, while several thousands of solid finite elements are used for the modeling of the rubber layers, the steel plates, the steel shims and also the lead core. Two alternative micro-models are formed and investigated, in an attempt to define the bounds of the effects of the lead core's confinement to the behavior of the bearing. The models are tested for vertical static loading followed by a horizontal cyclic loading and the distribution of strains, stresses and plastic zones within the bearing is studied. Also the lateral force-displacement curves obtained from the analytical study are compared to the respective simplified bilinear elastoplastic curve suggested by the manufacturer of the LRB.*

1 INTRODUCTION

The elastomeric Lead-Rubber Bearings (LRB), which are used for the base isolation of structures, generally consist of two fixing steel plates located at the top and bottom of the bearing, several alternating layers of elastomer and steel shims and a central lead core (Figure 1a). The elastomeric material provides the isolation component with lateral flexibility, the lead core provides the energy dissipation or damping component, while the internal steel shims provide the vertical load capacity of the bearing. The steel shims, together with the top and bottom steel fixing plates, also confine the central lead core. During the seismic excitation of the structure, the rubber layers deform laterally by shear deformation, allowing the structure to translate horizontally and absorbing energy when the lead core yields [1].

For the deformation and strength capacity control of each bearing part (rubber layers, lead core and steel shims) and for the different load conditions (vertical load, cyclic lateral loading, buckling control, etc.) that must be taken into account according to the Code Provisions [2], simple analytical formulas are used. These formulas are referred to a simplified model of the bearing, not necessarily the same for each design check.

Even for a more detailed description of the bearing's response to lateral loading, simple analytical models are also used, usually with one finite element and bilinear elastoplastic law with hardenind [3], or with two finite elements (one perfectly plastic and one unlimited elastic) in parallel conection [4]. In these models, the bearing's parameters that describe the lateral force–displacement bilinear law are the initial elastic stiffness K_u, the yielded stiffness K_d, the characteristic strength Q_d and the lateral design displacement D_d. Values for these parameters are acquired from the manufacturer of the bearing, so as to be in accordance with the elaborated results from a series of experimental tests, where the basic matching criterion is the equivalence of the hysteresis loop area between the experimental and the analytical model. They can also be predicted with remarkable accuracy by using simple analytical formulas, except from the initial elastic stiffness K_u value which is mainly a function of the fabrication details of the bearing and especially of the confinement of the lead core. It should be noted that limited only attempts of using finite element micromodels for the analysis of the LRBs are known to date and they mainly focus on determining the lateral force-displacement curves of the bearings [5].

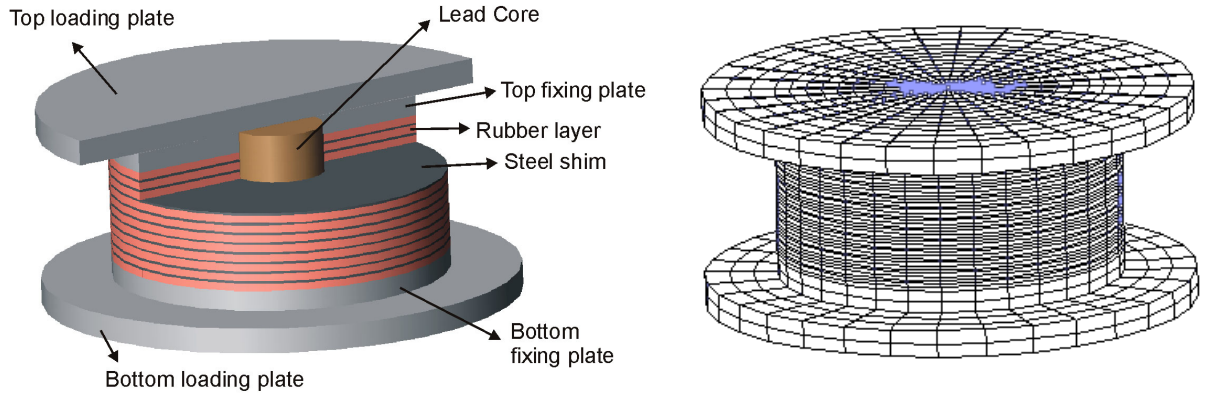

Figure 1. (a) Examined LRB, (b) Finite element micromodel

In this paper, the geometric shape of these bearings is modeled analytically by taking into account detailed fabrication drawings of a standard lead-rubber bearing, while several thousands of solid finite elements are used for the modeling of the rubber layers, the steel plates and shims and also the lead core. Two alternative micro-models are formed and investigated, in an attempt to define the bounds of the effects of the lead core's confinement. The models are tested for vertical static loading together with horizontal cyclic loading and the distribution of stresses and plastic strains within the bearing is studied. Also the lateral force-displacement curves obtained from the analytical study are compared to the respective simplified bilinear elastoplastic curve suggested by the manufacturer of the isolation bearing.

2 ANALYTICAL MODELING

The LRB under consideration is the Skellerup150 isolator, made by the Skellerup Industries[1] and shown in Figure 1a. The isolator consists of:

- 2 loading steel plates (top and bottom) with a 601 mm diameter and a 31,8 mm thickness,
- 2 fixing steel plates (top and bottom) with a 431 mm diameter and a 25,4 mm thickness,
- 11 rubber layers with a 431 mm diameter and a 9,5 mm thickness,
- 10 steel shims with a 431 mm diameter and a 3,0 mm thickness,
- a central lead core with a 116,8 mm diameter and a 185 mm height.

The basic technical specifications given by the manufacturer are as follows:

- design compressive load DCL=667 kN (150 kip),
- lateral design displacement D_d=0,1524 m,
- yielded stiffness K_d=858 kN/m,
- elastic stiffness K_u=11050 kN/m,
- lateral force (at D_d)= 251,3 kN.

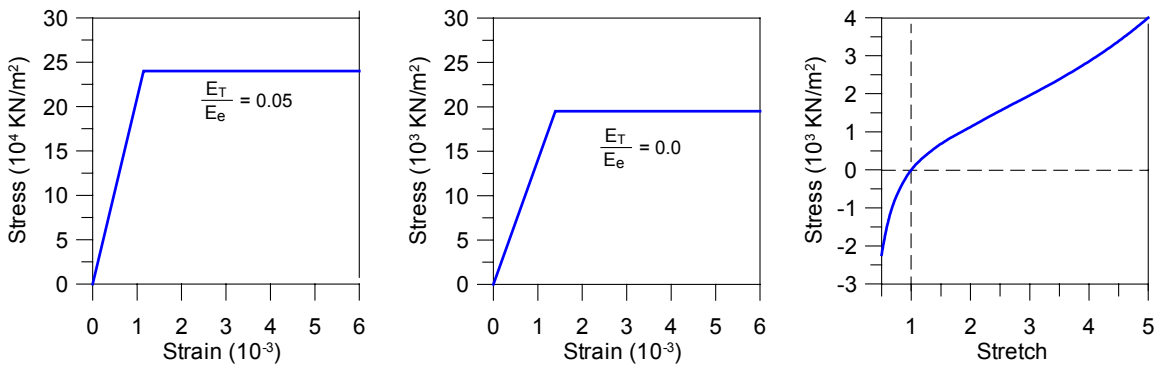

Figure 2. Stress-strain laws of the LRB materials

The proposed finite element model of the bearing (model-1) is shown in Figure 1b and includes 5632 solid hexaedron 8-node elements for the rubber layers, 2560 elements for the steel shims and 1440 elements for the lead core, to a total of 12448 elements and 14326 nodes. In model-1, full bond was assumed between the steel and rubber material. Also the lead core was assumed to be tightly fitted in the bearing [6], thus considering fixed boundary conditions to hold between the lead core and the steel shims and rubber layers. However, since the confinement of the core depends on the manufacturing details, a second alternative model (model-2) was formed, without any interaction between the lead core and the steel shims and rubber layers, in order to define the bounds of the effects of the core's confinement to the deformation and stress state of the bearing. In the later model the lead core was firmly connected only with the top and bottom fixing plates of the bearing.

The steel material of the top and bottom plates and the shims was assumed to be a mild steel with a Young modulus $E=21\times10^7$ kN/m, Poisson's ratio $\nu=0,30$, bilinear elastoplastic constitutive law (Figure 2a) with 5% strain hardening ratio and a Von Mises yield criterion with $\sigma_y=240\times10^3$ kN/m^2 (uniaxial). The lead core was assumed to have a Young modulus $E=18\times10^6$ kN/m, Poisson's ratio $\nu=0,43$, bilinear elastoplastic constitutive law (Figure 2b) and a Von Mises yield criterion with $\sigma_y=19,5\times10^3$ kN/m^2 (uniaxial). For the rubber layers an hyper-elastic material law was considered (Figure 2c), according to the Arruda-Boyce constitutive model [7] which was properly modified in order to take into consideration the finite compressibility of the rubber. This model requires two material constants, the initial shear modulus G_o and the locking stretch λ_m. The material constants of the rubber were estimated according to AASHTO 1999 Guide Specifications [2] for natural rubber with hardness 50, taking the values G=620 kN/m^2 for the shear modulus and $K=15\times10^5$ kN/m^2 for the bulk modulus. In fact, an attempt was made to fairly estimate all the material constants related to this bearing, since they could not been found from the manufacturer of the bearing.

The examined models were subjected to 2 quasi-static loading sequences, corresponding to the design compressive load and the design lateral displacement suggested by the manufacturer. That is, a vertical compressive load with a maximum value of P=667 kN (150 kips) was applied in 10 steps, followed by a cycling imposed horizontal displacement with an amplitude of 0,1524 m (6 inches) applied in 120 steps, which results in a rubber's maximum shear strain of about 145%. The quasi-static analysis was performed by the computer code ADINA [8], taking into consideration the large strain and large displacement effects.

3 RESPONSE RESULTS TO QUASI-STATIC LOADING

In the following, some characteristic results of the system's response are presented and evaluated, beginning with the first stage of the loading process.

3.1 Vertical compressive loading

Figure 3 shows the distribution of the effective stresses within the lead core of the examined models, when applying 100% of the total vertical load. The stress state in both models is quite similar, while in the most of the core the effective stress has already reached the yielding stress of the lead, even before any additional lateral load was applied to the bearing. It should be noted that the first yielding took place at about 60% of the total vertical load, an event that is not yet sufficiently known, neither is taken into consideration by the simplified analytical models which are used for the LRBs.

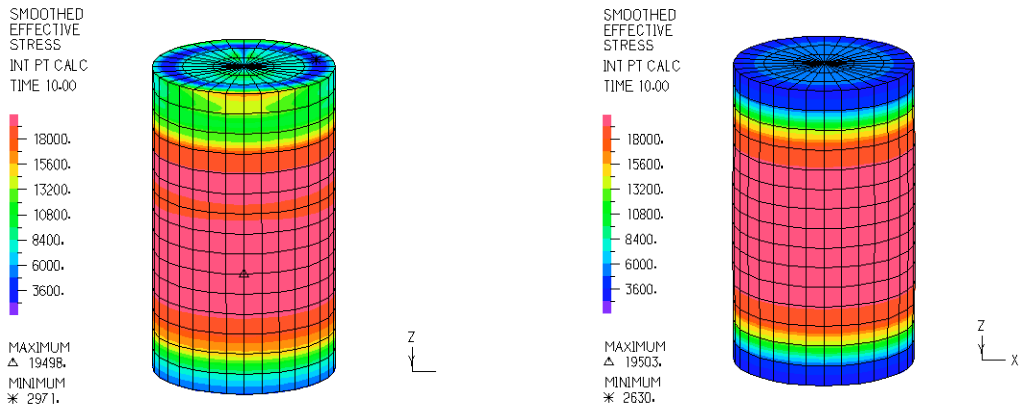

(a) model-1 (b) model-2

Figure 3. Effective stress within lead core for the maximum value of the vertical load.

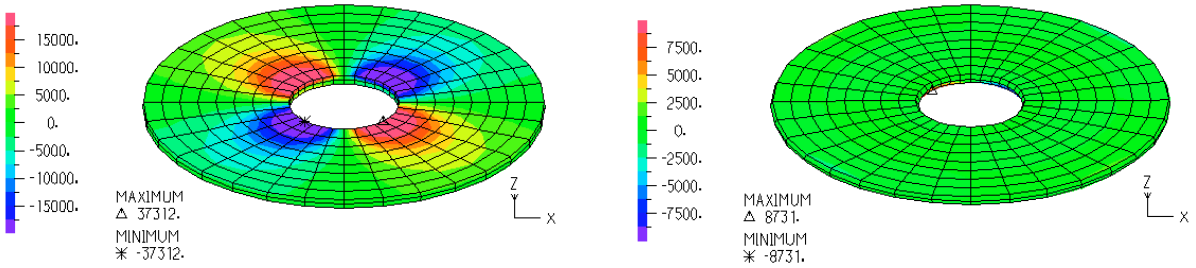

(a) model-1 (b) model-2

Figure 4. Horizontal shear stresses S_{xy} within the bottom rubber layer

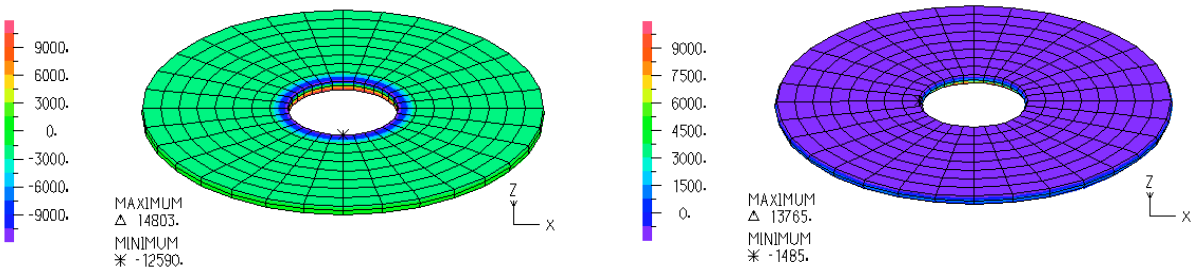

(a) model-1 (b) model-2

Figure 5. Hydrostatic pressure S_o within the bottom rubber layer

Figure 4 shows the distribution of horizontal shear stresses S_{xy} within the top face of the bottom rubber layer, corresponding to the 100% application of the total vertical load. It is observed that in model-1 the extreme shear stresses are about 4 times greater than in model-2, which means that the tight fitting of the lead core in model-1 causes a high concentration of rubber shear stresses around the hole of the layer.

Figure 5 shows the distribution of hydrostatic pressure S_o within the top face of the bottom rubber layer, for the 100% application of the total vertical load. The maximum positive pressure (compression) is quite similar in both models and is located around the central hole at the bottom face of the layer. However, in model-1 the minimum negative pressure (tension) is many times greater than in model-2 and is located at an area around the central hole at the top face of the layer. This area is critical for the control of the bond strength between the rubber layers and the steel shims. This stress concentration, shown in Figures 4a and 5a, cannot be predicted by the simplified analytical models which are used for the LRBs.

3.2 Horizontal cycling loading

After the application of the vertical commpressive load, a cycling imposed horizontal displacement with an amplitude of ±0,1524 m (6 inches) was applied into 120 steps. In Figure 6 the deformed shape of the compared models is shown when the horizontal displacement takes its maximum value U_{xmax}=0,1524 m. The deformed shape of the compared models is very similar, except from the left corner of the top rubber layer, where the deformation of model-2 is considerably greater than that of model-1. The largest deformation of the rubber develops at the right corner of the bottom rubber layer.

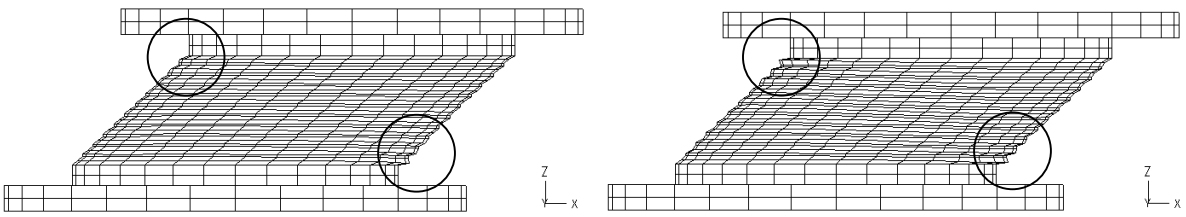

(a) model-1 (b) model-2

Figure 6. Deformed shapes of examined models for max imposed horizontal displacement

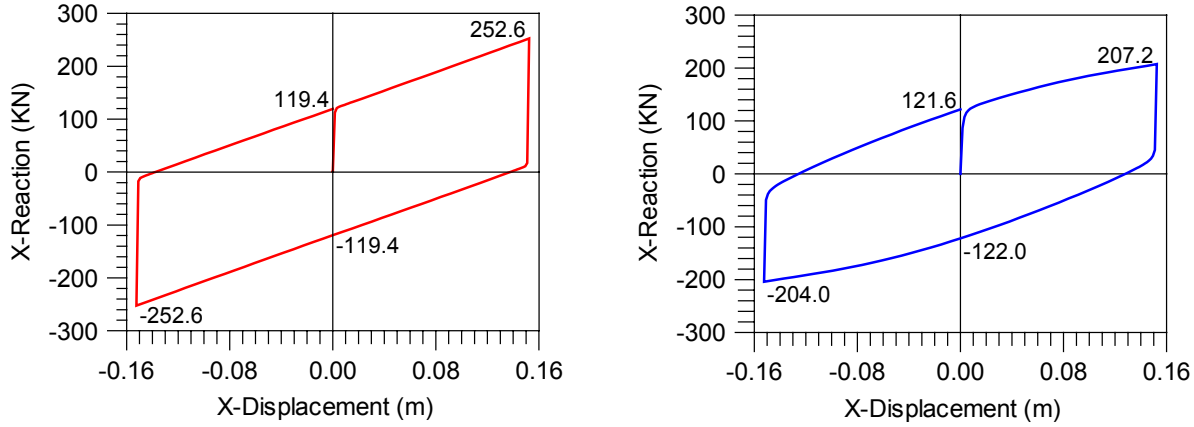

(a) model-1 (b) model-2

Figure 7. Force-displacement diagrams of the examined models

Figure 7 shows the horizontal force-displacement curves of the examined models during the entire loading cycle. It is observed that the characteristic strength of model-1 (119,4 kN) is about equal to the strength of model-2 (121,8 kN), which means that the confinement of the lead core very little affected the characteristic strength of the compared models. It is also observed that the maximum horizontal force of model-2 is about 20% less than the respective force of model-1 and the area of hysteresis loop of model-2 (indicating the energy loss per cycle) is about 8,0% less than the area of model-1. These observations denote that the confinement of the lead core affects significantly the size of the maximum horizontal force, but affects less the energy dissipation properties of the bearing. In conclusion, the bilinear form of the force-displacement curve resulted from model-1 indicates the perfect confinement of the lead core.

In Figure 8 the deformed shape of the lead core, as well as the distribution of the effective stresses within the core is shown, due to the maximum value of the imposed horizontal displacement. In both models a significant stretching of the lead core is observed, not only in shear but in elongation too. It is noted that this elongation cannot be accurately described without considering large displacement effects in the finite element analysis. It is also noted that the deformed shape of the lead core of model-2 is highly incompatible to the deformed shape of the rubber layers and steel shims, thus concluding that model-2 is suitable only for comparison purposes with the more precise model-1. Regarding the distribution of the effective stresses, it is very similar in both models. Namely, the effective stresses have reached the yielding stress over the whole height of the core, except from the top and bottom ends which are firmly connected with the respective steel fixing plates.

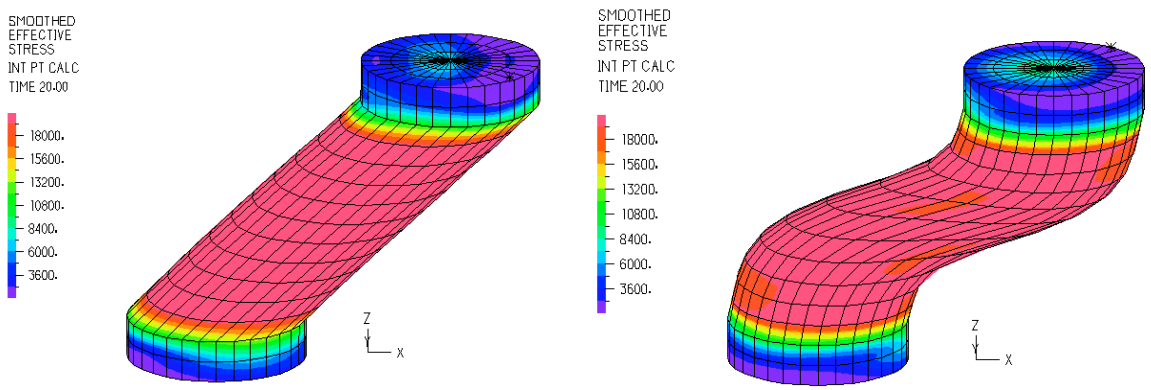

(a) model-1 (b) model-2

Figure 8. Deformed shape and effective stresses in lead core due to max imposed horizontal displacement

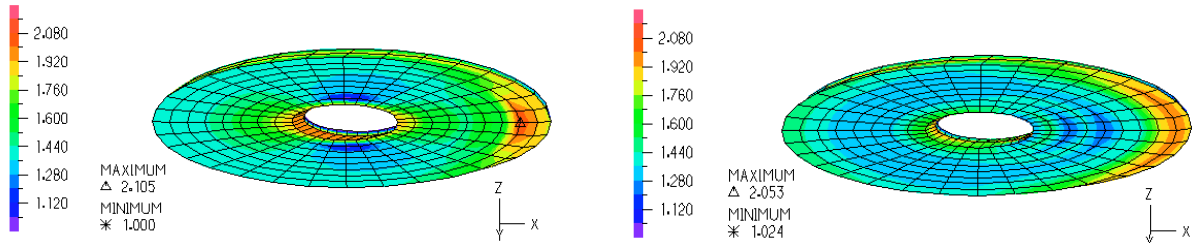

(a) model-1 (b) model-2

Figure 9. Maximum principal strains at the bottom rubber layer

Figures 9, 10 and 11 are related to the deformation and stress state in the bottom rubber layer, due to the maximum value (+0,1524 m) of the imposed horizontal displacement. In particular, Figure 9 shows the distribution of the maximum principal strains at the bottom face of this layer. It can be seen that the largest values of the strains are about 40% higher than the mean shear strains of the bearing's rubber layers (which have been previously estimated to 145%) and are located around the central hole and near the right boundary of the layer.

Figure 10 shows the distribution of the horizontal shear stresses S_{xz} within the rubber layer. It is observed that in model-2 the stress distribution is fairly smooth, while in model-1 the stress distribution contains large positive and negative peak values. The maximum values in model-1 are about 4 times greater than the maximum values in model-2 and the minimum values in model-1 are more than 20 times greater than in model-2. This non-smooth distribution of shear stresses S_{xz} within the rubber layer of model-1 is obviously due to the tight fitting of the lead core in this model.

Figure 11 shows the distribution of hydrostatic pressure S_o within the rubber layer. It is observed that the pressure distribution is significantly different within the compared models, as well as the location of the maximum (compressive) pressure values. In conclusion, the confinement of the lead core significantly affects the distribution and the size of the stresses within the rubber layers. Moreover, the non-smooth stress distribution in model-1, as shown in Figures 10a and 11a, cannot be predicted by the simplified analytical models which are used for the LRBs.

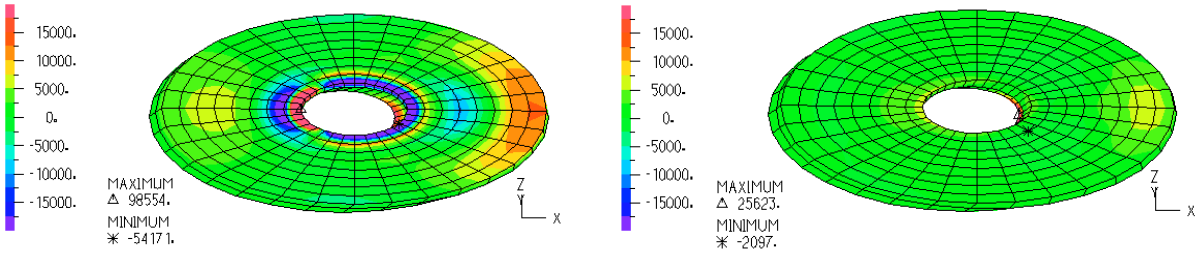

(a) model-1 (b) model-2

Figure 10. Horizontal shear stresses S_{xz} within bottom rubber layer

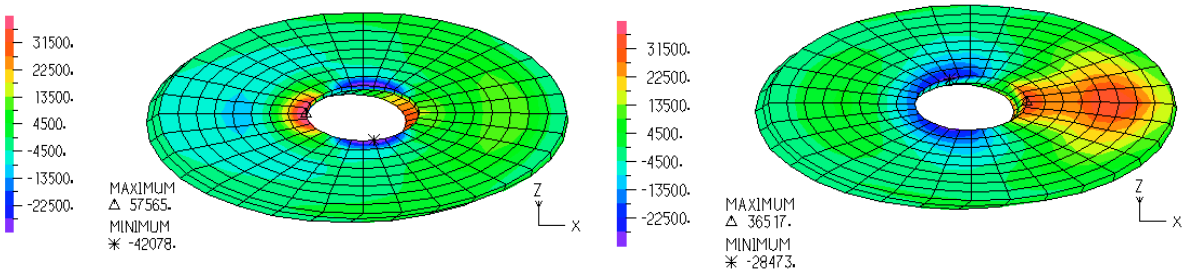

(a) model-1 (b) model-2

Figure 11. Hydrostatic pressure within bottom rubber layer

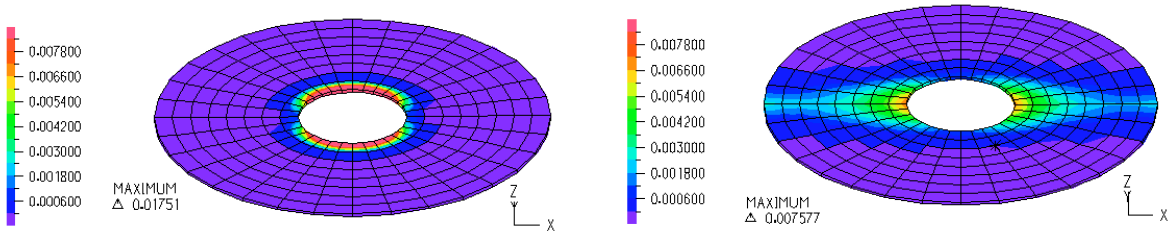

(a) (b)

Figure 12. Total accumulated effective plastic strains within the middle steel shim

Figure 12 shows the distribution of the accumulated effective plastic strains within the middle steel shim of the bearing, at the end of the cycling loading process. The plastic strains in model-1 take values more than twice larger than those in model-2 and are strictly located around the central hole of the shim, while in model-2 they are distributed in a strip along the x-x diameter of the shim. The development of plastic strains in model-2 is due to the low yield strength of the mild steel. However, the development of plastic strains in model-1 is mainly due to the lateral strong interaction between the steel shims and the lead core. This conclusion has been assured by analyzing a model similar to model-1, but with a twice higher strength in the steel shims.

Figure 13 shows the vertical distribution of plastic zones within the steel shims, as well as the lateral interaction between the shims and the core of the model-1, due to the maximum value (+0,1524 m) of the imposed horizontal displacement. When reversing the imposed horizontal displacement (–0,1524 m), the shape of the core-shims' interaction also changes and finally, at the end of the cyclic loading process, accumulative plastic strains have developed in all the steel shims of the LRB.

The horizontal force-displacement curves of the examined models during the entire loading cycle, are comparatively shown in Figure 14a, together with the respective simplified bilinear elastoplastic curve suggested by the manufacturer of the isolation bearing (model-3). It is evident that the characteristic strengths of the compared three models, as well as the entire curves of model-1 and model-3, practically coincide, except from their unloading parts, where the unloading stiffness of model-3 is considerably less than the unloading stiffness of model-1 and model-2. Consequently, the area of hysteresis loop of model-1 is about 7,0% more than the area of model-3, while the area of hysteresis loop of model-2 is about 1,0% less than the area of model-3. It must be noted that the unloading stiffness (which is equal to the initial elastic stiffness K_u) suggested by the manufacturer, has not been established directly by the experimental tests of this bearing (Figure 14b). The unloading stiffness obtained by these tests is quite similar to the unloading stiffness obtained by the examined model-1 and model-2.

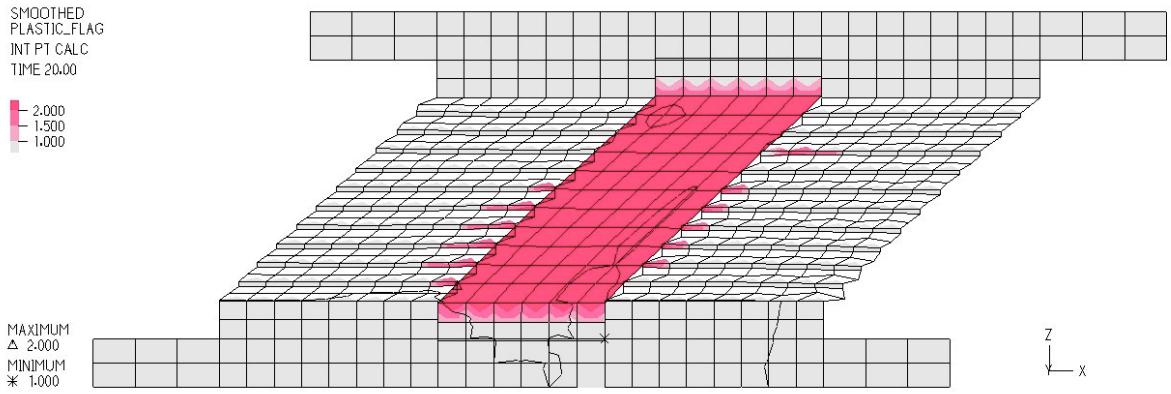

Figure 13. Distribution of plastic zones (red color) in a meridian x-x section.

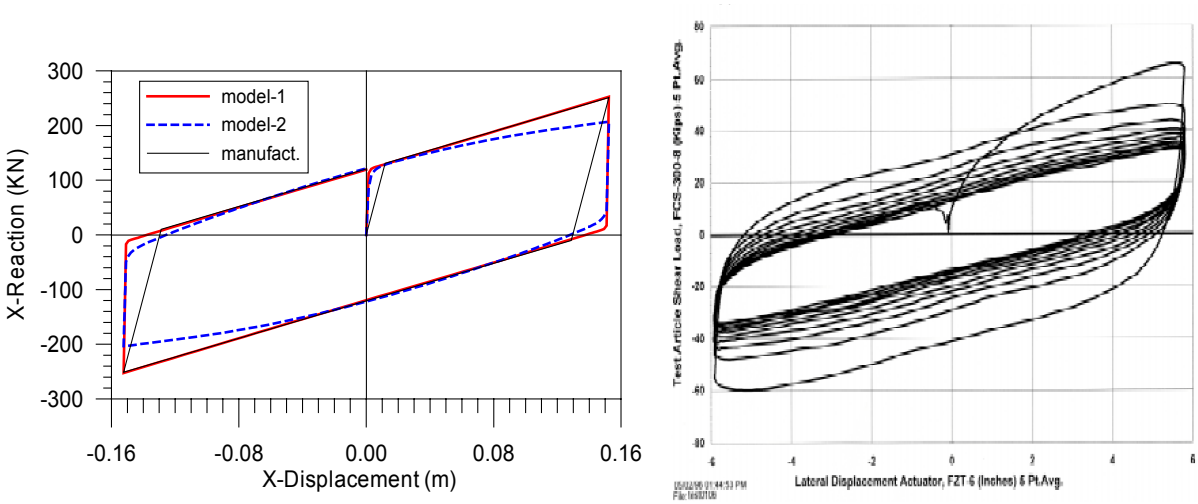

(a) Analytical models (kN, m) (b) Experimental results (kip, in)

Figure 14. Force-displacement curves' comparison between analytical and experimental results

4 CONCLUSIONS

The finite element micromodels provide increased possibilities for a more detailed study of the stress, strain and available strength of LRBs. In this way, a better understanding of their mechanical behavior is possible, by detecting their critical areas and thus contributing to the improvement of their design.

Concerning the examined structural system, it must be noted that the existence of the lead core causes a significant disturbance on the smooth distribution of the stresses and strains in the interior of the bearings, so the use of micromodels in the study of LRBs would be advisable.

It must be noted also that for the validity of the quantitative conclusions obtained for the examined LRB, it is necessary to verify the basic assumptions that have been made, which concern its material properties and fabrication details.

ACKNOWLEDGEMENTS

A part of this report is based on research sponsored by the European Commission and the Ministry of National Education and Religions Affairs of Greece (within the framework of the Operational Programme of Education and Initial Vocational Training – Ε.Π.Ε.Α.Ε.Κ.).

REFERENCES

[1] "Evaluation findings for skellerup base isolation elastomeric bearings" (1998), Technical evaluation report, (CERF report: HITEC 98-12), prepared by the Highway Innovative Technology Evaluation Center.
[2] AASHTO, American Association of State Highway Transportation Officials (1999), "Guide Specifications for Seismic Isolation Design" , Washington D.C.
[3] SAP2000: "Integrated Finite Element Analysis and Design of Structures" (1999), Computers and Structures, Inc., Berkeley, USA.
[4] Kelly T. E. (2001), "Base isolation of Structures- Design Guidelines", Holmes Consulting Group Ltd, Wellington, New Zealand.
[5] Ali, H. M. and Abdel-Ghaffar, A. M. (1995), "Modeling of rubber and lead passive-control bearings for seismic analysis", J. Struct. Engrg., ASCE, Vol. 121 (7), 1134-1144.
[6] Naeim F, Kelly J. (1999), "Design of seismic isolated structures". John Wiley & Sons, Inc.
[7] Arruda E. M. and Boyce M. C. (1993), "A three-dimensional constitutive model for the large stretch behavior of rubber elastic materials", J. Mech. Phys. Solids, Vol. 41 (2), 389-412.
[8] ADINA: "Automatic Dynamic Incremental Nonlinear Analysis" (2003), Adina R&D, Inc., Watertown, USA.